Creating vortons and three-dimensional skyrmions from domain-wall annihilation with stretched vortices in Bose-Einstein condensates

Muneto Nitta,[1] Kenichi Kasamatsu,[2] Makoto Tsubota,[3] and Hiromitsu Takeuchi[4]

[1]*Department of Physics, and Research and Education Center for Natural Sciences, Keio University, Hiyoshi 4-1-1, Yokohama, Kanagawa 223-8521, Japan*

[2]*Department of Physics, Kinki University, Higashi-Osaka, 577-8502, Japan*

[3]*Department of Physics, Osaka City University, Sumiyoshi-Ku, Osaka 558-8585, Japan*

[4]*Graduate School of Integrated Arts and Sciences, Hiroshima University, Kagamiyama 1-7-1, Higashi-Hiroshima 739-8521, Japan*

(Received 22 March 2012; published 25 May 2012)

We study a mechanism to create a vorton or three-dimensional skyrmion in phase-separated two-component BECs with the order parameters Ψ_1 and Ψ_2 of the two condensates. We consider a pair of a domain wall (brane) and an antidomain wall (antibrane) stretched by vortices (strings), where the Ψ_2 component with a vortex winding is sandwiched by two domains of the Ψ_1 component. The vortons appear when the domain wall pair annihilates. Experimentally, this can be realized by preparing the phase separation in the order Ψ_1, Ψ_2, and Ψ_1 components, where the nodal plane of a dark soliton in Ψ_1 component is filled with the Ψ_2 component with vorticity. By selectively removing the filling Ψ_2 component gradually with a resonant laser beam, the collision of the brane and antibrane can be made, creating vortons.

DOI: 10.1103/PhysRevA.85.053639 PACS number(s): 03.75.Lm, 03.75.Mn, 11.25.Uv, 67.85.Fg

I. INTRODUCTION

Quantized vortices are one of remarkable consequences of superconductivity and superfluidity. In multicomponent superfluids and superconductors, there appear many kinds of exotic vortices. When a vortex of one condensate traps another condensate inside its core, a supercurrent or superflow of the latter can exist along the vortex line. Such a vortex is called a superconducting or superflowing cosmic string in cosmology [1]. Because of the Meissner effect, superconducting strings exclude magnetic fields like superconductive wires, so that they are proposed to explain several cosmological phenomena related to galactic magnetic fields. When a superconducting string is closed and "twisted," that is, when the second condensate inside the string core has a nontrivial winding along the string loop, the supercurrent persistently flows along the loop and makes it stable. Such a twisted vortex loop is called a "vorton," a particle-like soliton made of a vortex [2,3]. While vortons were discussed in ^{3}He superfluids [4], they are considered to be a candidate of dark matter, and a possible source of ultrahigh energy cosmic ray. There have been a lot of study about their stability, interaction, and applications to cosmology [5].

On the other hand, three-dimensional (3D) skyrmions are topological solitons (textures) characterized by the third homotopy group $\pi_3(\mathrm{SU}(2)) \simeq \mathbf{Z}$ in a pion effective field theory. Skyrmions were proposed to be baryons [6]. Since their proposal, the skyrmions have been studied for a long time about their stability, interaction, and applications to nuclear physics [7].

Both 3D skyrmions and vortons have been fascinating subjects in high energy physics and cosmology for decades, and a lot of work have been done already, but they have yet to be observed in nature. On the other hand, these topological excitations, 3D skyrmions [8–14] and vortons [15,16], can be realized in Bose-Einstein condensates (BECs) of ultracold atomic gasses. Moreover 3D skyrmions and vortons have been shown to be topologically equivalent in two-component BECs [8,9]. BECs are extremely flexible systems for studying solitons (or topological defects) since optical techniques can be used to control and directly visualize the condensate wave functions [17]. Interest in various topological defects in BECs with multicomponent order parameters has been increasing; the structure, stability, and creation and detection schemes for monopoles [18–21], knots [22], and non-Abelian vortices [23] have been discussed [24].

It is, however, still unsuccessful to create vortons and 3D skyrmions experimentally, although the schemes to create and stabilize them have been theoretically proposed [8–14]. In the present study we propose how to create vortons or 3D skyrmions in two-component BECs from domain walls and quantized vortices. Specific examples of the system include a BEC mixture of two-species atoms such as ^{87}Rb-^{41}K [25] or ^{85}Rb-^{87}Rb [26], where the miscibility and immiscibility can be controlled by tuning the atom-atom interaction via Feshbach resonances. Here the domain wall is referred to as an interface boundary of phase-separated two-component BECs. Although the interface has a finite thickness, the wall is well-defined as the plane in which both components have the same amplitude. Since a description of two-component BECs can be mapped to the O(3) nonlinear sigma model (NLσM) by introducing a pseudospin representation of the order parameter [27–29], the resultant wall-vortex composite soliton corresponds to the Dirichlet (D)-brane soliton described in Refs. [30–34], which resembles a D-brane in string theory [35–37]. Such a D-brane soliton has been already numerically constructed by us in two-component BECs [38]. We have found that these composite solitons are energetically stable in rotating, trapped BECs and are experimentally feasible with realistic parameters. Similar configuration has been also studied in spinor BECs [39].

A brane-antibrane annihilation was demonstrated to create some topological defects in superfluid ^{3}He [40]. However, a physical explanation of the creation mechanism of defects still remains unclear. The intriguing experiment that mimicked

the brane-antibrane annihilation was performed in cold atom systems with the order parameters Ψ_1 and Ψ_2 of two-component BECs by Anderson *et al.* [41]. They prepared the configuration of the phase separation in the order Ψ_1, Ψ_2, and Ψ_1 components, where the nodal plane of a dark soliton in one component was filled with the other component. By selectively removing the filling component with a resonant laser beam, they made a planer dark soliton in a single-component BEC. Then, the planer dark soliton in 3D system is dynamically unstable for its transverse deformation (known as snake instability) [41], which results in the decay of the dark soliton into vortex rings. In the two-component BECs we have numerically simulated brane-antibrane annihilations, which resulted in vortex loops [42].

In this paper we consider a junction of a D-brane soliton and its antisoliton, namely a pair of a domain wall and an antidomain wall stretched by vortices. We give an approximate analytic solution for a pair of the D-brane and anti-D-brane in the O(3) NLσM. We show that this unstable configuration decays into a vorton or a 3D skyrmion, instead of an untwisted vortex ring [41] in the case without stretched vortices. Experimentally this can be realized by preparing the phase separation in the order Ψ_1, Ψ_2, and Ψ_1 components, and rotating the intermediate Ψ_2 component. By selectively removing the filling Ψ_2 component gradually with a resonant laser beam, the collision of the D-brane and anti-D-brane can be made, to create vortons.

This paper is organized as follows. In Sec. II we present the Gross-Pitaevski energy functional of two-component BECs, and rewrite it in the form of NLσM. In Sec. III, after constructing a phase separation, that is, a domain wall configuration in NLσM, we consider a pair of a domain wall and an antidomain wall. We discuss a creation of vortex in two dimensions, and a creation of vortex loops in three dimensions after a pair annihilation of the domain walls. In Sec. IV we consider a pair of a domain wall and an antidomain wall with vortices stretched between them. We show that when a vortex loop encloses n of the stretched vortices, the phase of the Ψ_2 component winds n times, that is, it is a vorton with n twist. We also confirm a vorton with $n = 1$ is topologically equivalent to a 3D skyrmion. Section V is devoted to a summary and discussion.

II. SYSTEM

A. Gross-Pitaevski energy functional

The order parameter of two-component BECs is

$$\mathbf{\Psi} = (\Psi_1, \Psi_2), \tag{1}$$

where

$$\Psi_j = \sqrt{\rho_j} e^{i\theta_j} \ (j = 1,2) \tag{2}$$

are the macroscopically occupied spatial wave function of the two components with the density ρ_j and the phase θ_j. The order parameter can be represented by the pseudospin

$$\mathbf{s} = (s_1, s_2, s_3) = (\sin\theta\cos\phi, \sin\theta\sin\phi, \cos\theta) \tag{3}$$

with a polar angle $\theta = \cos^{-1}[(\rho_1 - \rho_2)/\rho]$ and an azimuthal angle $\phi = \theta_2 - \theta_1$ as

$$\mathbf{\Psi} = \sqrt{\rho} e^{i\frac{\Theta}{2}} \left(\cos\frac{\theta}{2} e^{-i\frac{\phi}{2}}, \sin\frac{\theta}{2} e^{i\frac{\phi}{2}} \right), \tag{4}$$

where $\rho = \rho_1 + \rho_2$ and $\Theta = \theta_1 + \theta_2$ represent the local density and phase, respectively [27].

The solutions of the solitonic structure in two-component BECs are given by the extreme of the Gross-Pitaevski (GP) energy functional

$$E[\mathbf{\Psi}] = \int d^3x \left\{ \sum_{j=1,2} \left[\frac{\hbar^2}{2m_j} |\nabla\Psi_j|^2 + (V_j - \mu_j)|\Psi_j|^2 + \frac{g_{jj}}{2}|\Psi_j|^4 \right] + g_{12}|\Psi_1|^2|\Psi_2|^2 \right\}. \tag{5}$$

Here m_j is the mass of the jth component and μ_j is its chemical potential. The BECs are confined by the harmonic trap potential

$$V_j = \tfrac{1}{2} m_j \left(\omega_x^2 x^2 + \omega_y^2 y^2 + \omega_z^2 z^2 \right). \tag{6}$$

The coefficients g_{11}, g_{22}, and g_{12} represent the atom-atom interactions. They are expressed in terms of the s-wave scattering lengths a_{11} and a_{22} between atoms in the same component and a_{12} between atoms in the different components as

$$g_{jk} = \frac{2\pi\hbar^2 a_{jk}}{m_{jk}} \tag{7}$$

with $m_{jk}^{-1} = m_j^{-1} + m_k^{-1}$. The GP model is given by the mean-field approximation for the many-body wave function and provides quantitatively good description of the static and dynamic properties of the dilute-gas BECs [43].

B. Mapping to the nonlinear sigma model

To derive the generalized NLσM for two-component BECs from the GP energy functional (5), we assume $m_1 = m_2 = m$ and $V_1 = V_2 = V$. By substituting the pseudospin representation Eq. (4) of $\mathbf{\Psi}$, we obtain [27]

$$E = \int d^3x \left\{ \frac{\hbar^2}{2m} \left[(\nabla\sqrt{\rho})^2 + \frac{\rho}{4} \sum_{\alpha=1}^{3} (\nabla s_\alpha)^2 \right] + V\rho + \frac{m\rho}{2} |\mathbf{v}_{\rm eff}|^2 + c_0 + c_1 s_3 + c_2 s_3^2 \right\}, \tag{8}$$

where we have introduced the effective superflow velocity

$$\mathbf{v}_{\rm eff} = \frac{\hbar}{2m} (\nabla\Theta - \cos\theta\nabla\phi) \tag{9}$$

and the coefficients

$$c_0 = \frac{\rho}{8}[\rho(g_{11} + g_{22} + 2g_{12}) - 4(\mu_1 + \mu_2)], \tag{10}$$

$$c_1 = \frac{\rho}{4}[\rho(g_{11} - g_{22}) - 2(\mu_1 - \mu_2)], \tag{11}$$

$$c_2 = \frac{\rho^2}{8}(g_{11} + g_{22} - 2g_{12}). \tag{12}$$

The coefficient c_1 can be interpreted as a longitudinal magnetic field that aligns the spin along the x^3 axis; it was assumed

to be zero in this study. The term with the coefficient c_2 determines the spin-spin interaction associated with s_3; it is antiferromagnetic for $c_2 > 0$ and ferromagnetic for $c_2 < 0$ [27]. Phase separation occurs for $c_2 < 0$, which we are focusing on. Further simplification can be achieved by assuming that $V = 0$ and the total density is uniform through the relation $\rho = \mu/g$, where $g = g_{11} = g_{22}$ and $\mu = \mu_1 = \mu_2$, and that the kinetic energy associated with the superflow $\mathbf{v}_{\rm eff}$ is negligible. Although the assumptions $\mathbf{v}_{\rm eff} = 0$ and $\rho = \text{const}$ become worse in the vicinities of vortex cores or domain walls, this simplification does not affect later discussions about the vorton nucleations based on topology.

By using the healing length $\xi = \hbar/\sqrt{2mg\rho}$ as the length scale, the total energy can reduce to

$$\tilde{E} = \frac{E}{g\rho\xi^3} = \int d^3x \frac{1}{4}\left[\sum_{\alpha=1}^{3}\left(\nabla s_\alpha\right)^2 + M^2\left(1 - s_3^2\right)\right], \quad (13)$$

$$M^2 = \frac{4|c_2|}{g\rho^2}, \quad (14)$$

where M is the effective mass for s_3. This is a well-known massive NLσM for effective description of a Heisenberg ferromagnet with spin-orbit coupling.

Introducing a stereographic coordinate

$$u = \frac{s_1 - is_2}{1 - s_3}, \quad (15)$$

we can rewrite Eq. (13) as

$$\tilde{E} = \int d^3x \frac{\sum_{\alpha=1}^{3}|\partial_\alpha u|^2 + M^2|u|^2}{(1+|u|^2)^2}. \quad (16)$$

Here $u = 0$ (∞) corresponds to the south (north) pole of the S^2 target space.

III. WALL-ANTIWALL ANNIHILATION

A. Domain walls

For a domain wall perpendicular to the x^1 axis, $u = u(x^1)$, the total energy is bounded from below by the Bogomol'nyi-Prasad-Sommerfield (BPS) bound as [30,32,33,38]

$$\tilde{E} = \int d^3x \frac{|\partial_1 u \mp Mu|^2 \pm M(u^*\partial_1 u + u\partial_1 u^*)}{(1+|u|^2)^2} \geqslant |T_{\rm w}| \quad (17)$$

by the topological charge that characterizes the wall:

$$T_{\rm w} = M\int d^3x \frac{u^*\partial_1 u + u\partial_1 u^*}{(1+|u|^2)^2}, \quad (18)$$

where ∂_i denotes the differentiation with respect to x^i. Among all configurations with a fixed boundary condition, that is, with a fixed topological charge $T_{\rm w}$, the most stable configurations with the least energy saturate the inequality (17) and satisfy the BPS equation

$$\partial_1 u \mp Mu = 0, \quad (19)$$

which is obtained by $|\cdots|^2 = 0$ in Eq. (17). This equation immediately gives the analytic form of the wall configuration

$$u_{\rm w}(x^1) = e^{\mp M(x^1 - x_0^1) - i\phi_0}. \quad (20)$$

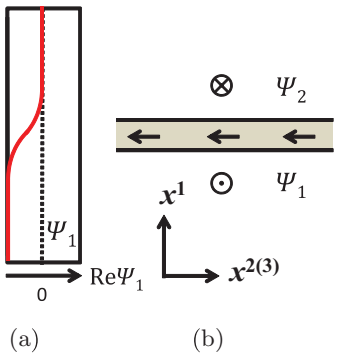

FIG. 1. (Color online) A single domain wall in two-component BECs. (a) The amplitude of Ψ_1 for a domain wall. (b) The pseudospin texture of the single domain wall perpendicular to the x^1 axis in real space. The arrows denote points in the target space S^2. The gradient and interaction energies are localized around the wall, which is shaded schematically. The arrows on the wall imply the phase ϕ_0 which the wall possesses.

The function $u_{\rm w}$ represents the domain wall with wall position x_0^1 and phase ϕ_0 associated with (s_1,s_2); this phase ϕ_0 yields the Nambu-Goldstone mode localized on the wall, as in Fig. 1. The sign $\mp$ implies a domain wall and an antidomain wall. The domain wall can be mapped to a path in the target space as shown in Fig. 2(a).

B. Wall-antiwall annihilation

As described in Sec. I, we note that the intriguing experiment that mimicked the brane–antibrane annihilation was performed by Anderson *et al.* [41]. They created the configuration shown in Fig. 3, where the nodal plane of a dark soliton in one component was filled with the other component. By selectively removing the filling component with a resonant laser beam, they made a planer dark soliton in a single-component BEC. The dark soliton corresponds to the coincident limit of the two kinks in Fig. 3(a). It

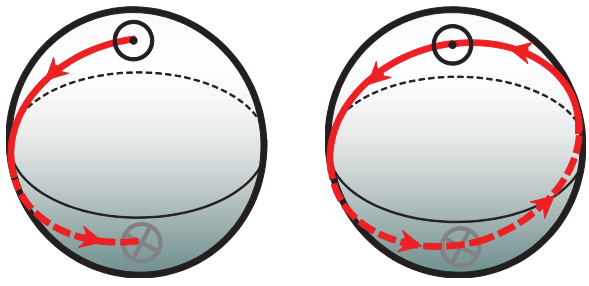

FIG. 2. (Color online) The S^2 target space where the north and south poles are denoted by $\odot$ and $\otimes$, respectively. (a) The path connecting the north and south poles represents the map from the path in the domain wall in Fig. 1(b) along the x^1 axis in real space from $x^1 \to -\infty$ to $x^1 \to +\infty$. The path in the S^2 target space passes through one point on the equator, which is represented by "$\leftarrow$" in Fig. 1(b) in this example. In general, the U(1) zero mode is localized on the wall. (b) The path in the target space S^2 for a domain wall and an antidomain wall. The path represents the map from the path along the x^1 axis from $x^1 \to -\infty$ to $x^1 \to +\infty$ in real space in Fig. 3(b).

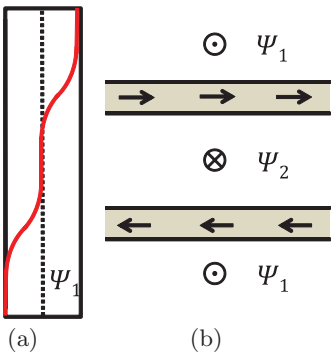

FIG. 3. (Color online) A pair of domain wall and antidomain wall in two-component BECs. (a) The amplitude of Ψ_1 for the wall and antiwall configuration. (b) The pseudospin texture of the wall and antiwall configuration in real space. The arrows denote the pseudospin. Ψ_1 (Ψ_2) is filled outside (between) the walls, where the other component is zero. In the upper (lower) region outside the walls, the phase of Ψ_1 is fixed to be zero (π).

is known that the planer dark soliton in the 3D system is dynamically unstable for its transverse deformation (known as snake instability) [41], which results in the decay of the dark soliton into vortex rings.

In our context, this experiment demonstrated the wall-antiwall collision and subsequent creation of cosmic strings, where the snake instability may correspond to "tachyon condensation" in string theory [44]. The procedure that removes the filling component can decrease the distance R between two domain walls and cause their collision. The tachyon condensation can leave lower dimensional topological defects after the annihilation of D-brane and anti-D-brane. In our case of the phase-separated two-component BECs, the annihilation of the two-dimensional defects (domain walls) leaves one-dimensional defects (quantized vortices).

Let us discuss this in two dimensions in more detail. Here U(1) zero modes of the wall and the antiwall are taken to be opposite as in Fig. 3(b). The configuration is mapped to a loop in the S^2 target space, see Fig. 2(b). This configuration is unstable. It should end up with the vacuum with the up-spin $\odot$. In the decaying process the loop is unwound from the south pole in the target space. To do this there are two topologically inequivalent ways, which are schematically shown in Figs. 4(a) and 4(b). In real space, at first, a bridge connecting two walls is created as in Figs. 4(c) and 4(d). Here there exist two possibilities of the spin structure of the bridge, corresponding to two ways of the unwinding processes. Along the bridge in the x^1 direction, the spin rotates (c) anticlockwise or (d) clockwise on the equator of the S^2 target space. Let us label these two kinds of bridges by "↓" and "↑", respectively.

In the next step, a "passage" through the bridge is formed as in Figs. 4(e) and 4(f), where the ground state, that is, the up-spin $\odot$ state, is filled between them. The phase of the filling Ψ_1 component through the passage is connected anticlockwise or clockwise [Figs. 4(g) and 4(h)] Let us again label these two kinds of passages by "↓" and "↑", respectively. In either case, the two regions separated by the domain walls are connected through a passage created in the decay of domain walls. Once created, these passages grow to holes in order to reduce the domain wall energy.

Several holes are created in the entire decaying process. Let us focus a pair of two neighboring holes. Then, one can

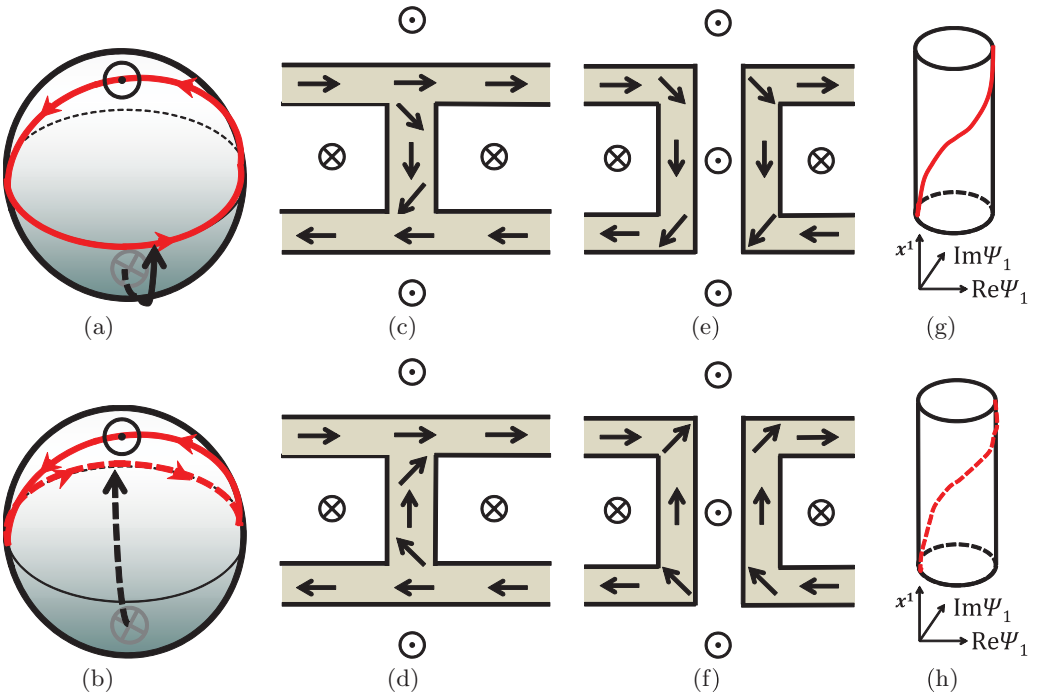

FIG. 4. (Color online) Decaying processes of the wall-antiwall pair. (a) and (b) The loop in the pseudospin space is unwound in two ways. (c) and (d) A bridge is created between the wall and antiwall. In this process there are two possibilities of spin structure along the bridge. (e) and (f) The upper and lower regions are connected with a passage through the bridge being formed. (g) and (h) The Ψ_1 component is filled inside the passage, and the phase of Ψ_1 component is connected anticlockwise or clockwise.

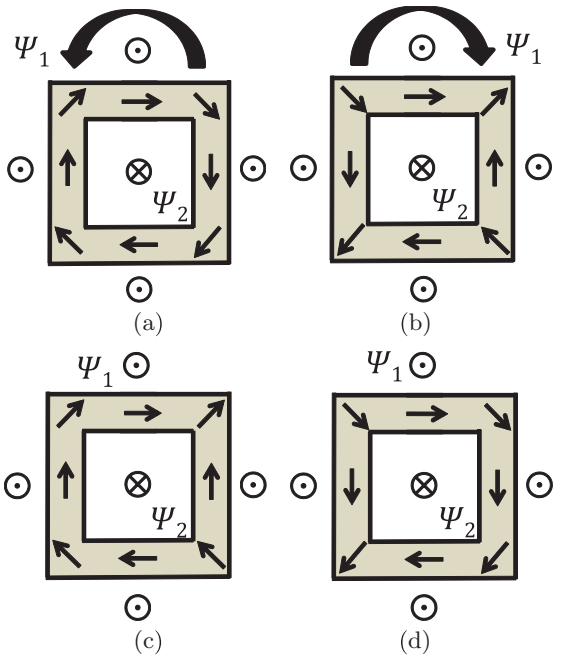

FIG. 5. (Color online) Stable and unstable wall rings. (a) and (b) Stable wall rings. The domain wall phase winds once (the winding number is ± 1) along the rings. Total configurations are 2D skyrmions with a nontrivial element ± 1 of the second homotopy group π_2. The phase Ψ_1 winds ± 1 so that it is a vortex, while Ψ_2 is filled inside the core. (c) and (d) Unstable wall rings. The domain wall phase does not wind (the winding number is 0) along the rings. The phase Ψ_1 does not wind so that it cannot be a vortex, while Ψ_2 is filled inside the ring. They decay into ground state (up pseudospin).

find a ring of a domain wall between the holes as shown in Fig. 5. Here, since there exist two kinds of holes ($\uparrow$ and $\downarrow$), there exist four possibilities of the rings, (a) $\uparrow\downarrow$, (b) $\downarrow\uparrow$, (c) $\uparrow\uparrow$, and (d) $\downarrow\downarrow$ in Fig. 5. In all the cases, the Ψ_2 component is confined in the domain wall rings. The phase of Ψ_1 component has a nontrivial winding outside the rings of types (a) and (b), whereas it does not have a winding outside the domain wall rings of types (c) and (d). Consequently, the domain wall rings of types (c) and (d) can decay and end up with the ground state $\odot$. However, the decay of the rings of types (a) and (b) is topologically forbidden; they are nothing but coreless vortices.

In the O(3) NLσM, the domain wall rings of types (a) of (b) are the Anderson-Toulouse vortices [45], or lumps in field theory [46]. The solutions can be written as ($z \equiv x^1 + ix^2$)

$$u = u_0 = \sum_{i=1}^{k} \frac{\lambda_i}{z - z_i} \quad \text{or} \quad u = \bar{u}_0 \tag{21}$$

for a lump or an antilump, where $z_i \in \mathbf{C}$ represent the position of the lump while and $\lambda_i \in \mathbf{C}^*$ with $|\lambda_i|$ and $\arg \lambda_i$ representing the size and the U(1) orientation of the lump, respectively. In fact, one can show that these configurations have a nontrivial winding in the second homotopy group $\pi_2(S^2) \simeq \mathbf{Z}$ which can be calculated from

$$\frac{1}{2\pi} \int d^2x \, \frac{i(\partial_1 u^* \partial_2 u - \partial_2 u^* \partial_1 u)}{(1 + |u|^2)^2}. \tag{22}$$

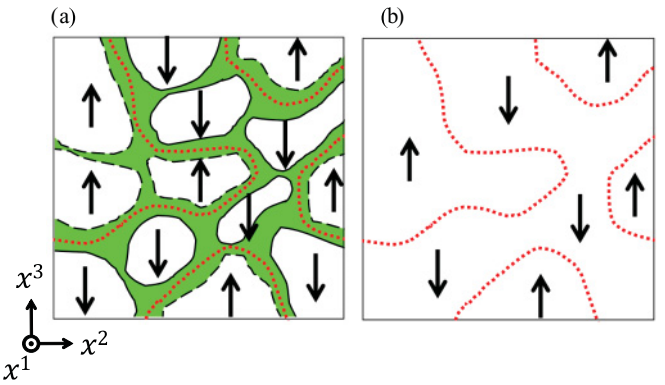

FIG. 6. (Color online) Decay of a domain wall pair in three dimensions. Domain walls are two-dimensional objects. (a) Two kinds of holes labeled by $\uparrow$ and $\downarrow$ are created after a domain-wall pair decay. (b) Along the boundary of these two kinds of holes, there appear vortex lines (denoted by dotted lines), which in general making vortex loops.

The wall rings of Figs. 5(a) and 5(b) belong to $+1$ and -1 of $\pi_2(S^2)$, respectively. Namely they are a lump and an antilump, respectively.

So far we have discussed two-dimensional space in which domain wall is a line and a vortex is point-like. In three dimensions, domain walls have two spatial dimensions. When the decay of the domain wall pair occurs, there appear two-dimensional holes, which can be labeled by $\downarrow$ or $\uparrow$ in Fig. 6(a). Along the boundary of these two kinds of holes, there appear vortex lines, which in general making vortex loops, as in Fig. 6(b). This process has been numerically demonstrated [42]. The vortex rings decay into the fundamental excitations in the end.

IV. D-BRANE–ANTI-D-BRANE ANNIHILATION

A. D-brane soliton

The D-brane soliton by Gauntlett *et al.* [30] can be reproduced in two-component BECs as follows [38]. For a fixed topological sector, vortices (a domain wall) parallel (perpendicular) to the x^1 axis, the total energy is bounded from below by the BPS bound as [30,32,33,38]

$$\begin{aligned} \tilde{E} &= \int d^3x \frac{|\partial_1 u \mp M u|^2 + |(\partial_2 \mp i\partial_3)u|^2}{(1 + |u|^2)^2} \\ &\pm \int d^3x \frac{M(u^*\partial_1 u + u\partial_1 u^*) + i(\partial_2 u^* \partial_3 u - \partial_3 u^* \partial_2 u)}{(1 + |u|^2)^2} \\ &\geqslant |T_{\rm w}| + |T_{\rm v}| \end{aligned} \tag{23}$$

by the topological charges that characterize the wall and vortices:

$$T_{\rm w} = M \int d^3x \frac{u^*\partial_1 u + u\partial_1 u^*}{(1 + |u|^2)^2}, \tag{24}$$

$$T_{\rm v} = i \int d^3x \frac{\partial_2 u^* \partial_3 u - \partial_3 u^* \partial_2 u}{(1 + |u|^2)^2}. \tag{25}$$

Then, the least energy configurations with fixed topological charges (a wall with a fixed number of vortices) satisfy the

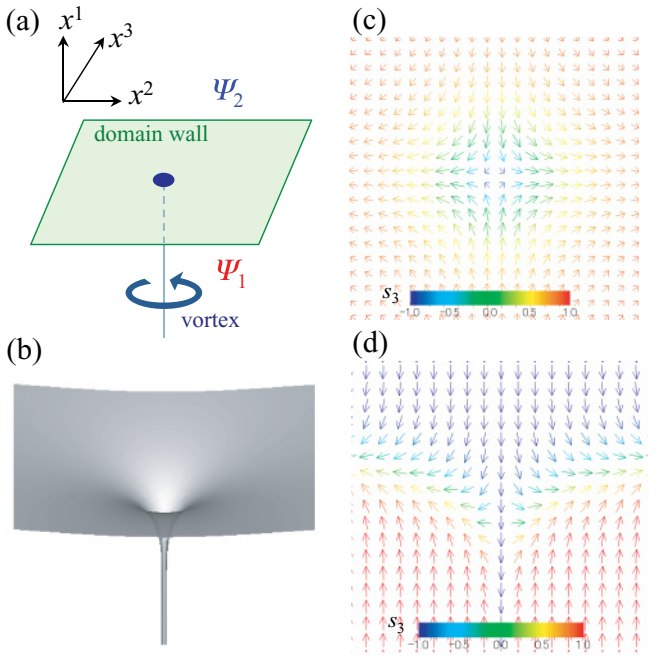

FIG. 7. (Color online) The typical D-brane soliton in two-component BECs. (a) Schematic illustration of the wall-vortex soliton configuration viewed from the length scale larger than the domain-wall width and the vortex core size. The two-component BECs Ψ_1 ($x^1 < 0$) and Ψ_2 ($x^1 > 0$) are separated by the domain wall. A single vortex located at $x^1 < 0$ (Ψ_1 component) is connected to the domain wall. (b) The isosurface of $s_3 = 0$ for the solution Eq. (27) of the NLσM, where $M = 1$, $x_0^1 = 0$, $\phi_0 = 0$, $N_{v1} = 1$, $N_{v2} = 0$, and $z_1^{(1)} = 0$. The corresponding spin textures $\mathbf{s}$ in the $z = 0$ plane and $y = 0$ plane are shown in (c) and (d), respectively. The magnitude of s_3 is denoted by color. We have $\mathbf{s} = (0,0,-1)$ along the vortex core.

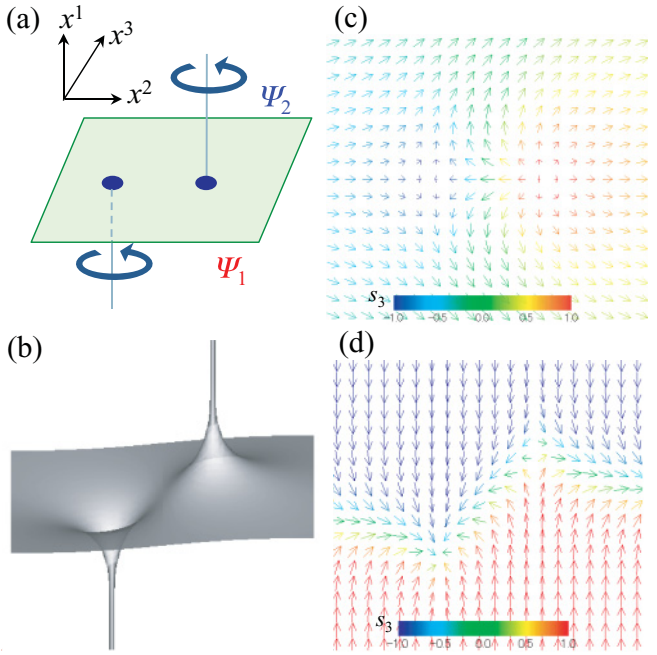

FIG. 8. (Color online) The D-brane soliton to which two vortices attach. (a) Schematic illustration of the configuration in which each component has a single vortex connected to the wall. (b) The isosurface of $s_3 = 0$ for the solution Eq. (27) of the NLσM, where $M = 1$, $x_0^1 = 0$, $\phi_0 = 0$, $N_{v1} = 1$, $N_{v2} = 1$, $z_1^{(1)} = -2$, and $z_1^{(2)} = 2$. The corresponding spin textures $\mathbf{s}$ in the $z = 0$ plane and $y = 0$ plane are shown in (c) and (d), respectively. The magnitude of s_3 is denoted by color. The wall becomes asymptotically flat due to the balance between the tensions of the attached vortices.

BPS equations

$$\partial_1 u \mp M u = 0, \qquad (\partial_2 \mp i\partial_3)u = 0. \tag{26}$$

The analytic form of the wall-vortex composite solitons can be found ($z \equiv x^2 + ix^3$)

$$u(x^1,z) = u_{\rm w}(x^1)u_{\rm v}(z), \tag{27}$$

where [32]

$$u_{\rm w}(x^1) = e^{\mp M(x^1 - x_0^1) - i\phi_0}, \tag{28}$$

$$u_{\rm v}(z) = \frac{\prod_{j=1}^{N_{v_1}} \left(z - z_j^{(1)}\right)}{\prod_{j=1}^{N_{v_2}} \left(z - z_j^{(2)}\right)}. \tag{29}$$

The function $u_{\rm w}$ represents the domain wall with wall position x_0^1 and phase ϕ_0. The function $u_{\rm v}$ gives the vortex configuration, being written by arbitrary analytic functions of z; the numerator represents N_{v_1} vortices in one domain (Ψ_1 component) and the denominator represents N_{v_2} vortices in the other domain (Ψ_2 component). The positions of the vortices are denoted by $z_j^{(1)}$ and $z_j^{(2)}$. The total energy does not depend on the form of the solution, but only on the topological charges as $T_{\rm w} = \pm M$ or 0 (per unit area), and $T_{\rm v} = 2\pi N_{\rm v}$ (per unit length), where $N_{\rm v}$ is the number of vortices passing through a certain $x^1 = $ const plane.

Figure 7 shows a D-brane soliton with the simplest wall-vortex configuration of Eq. (27). A vortex exists in $x^1 < 0$ and forms a texture, where the spin points down at the center and rotates continuously from down to up as it moves radially outward. The edge of vortex attaches to the wall, causing it to bend logarithmically as $x^1 = \log|z|/M$ [Figs. 7(b) and 7(d)]. We can construct solutions in which an arbitrary number of vortices are connected to the domain wall by multiplying by the additional factors $z - z_j^{(i)}$ [see Eq. (29)]; Fig. 8 shows a solution in which both components have one vortex connected to the wall. In the NLσM, the energy is independent of the vortex positions $z_j^{(i)}$ on the domain wall; in other words, there is no static interaction between vortices.

B. Brane-antibrane annihilation with a string

We are ready to study a pair of a domain wall and an antidomain wall stretched by vortices. An approximate analytic solution of the domain wall pair stretched by one vortex, which is schematically shown in Fig. 9(a), can be given in the O(3) NLσM as

$$u(x^1,z) = u_{\rm w}(x^1)u_{\rm v}(z), \tag{30}$$

$$u_{\rm w}(x^1) = e^{-M(x^1 - x_1^1) - i\phi_1} + e^{M(x^1 - x_2^1) - i\phi_2}, \tag{31}$$

$$u_{\rm v}(z) = 1/z. \tag{32}$$

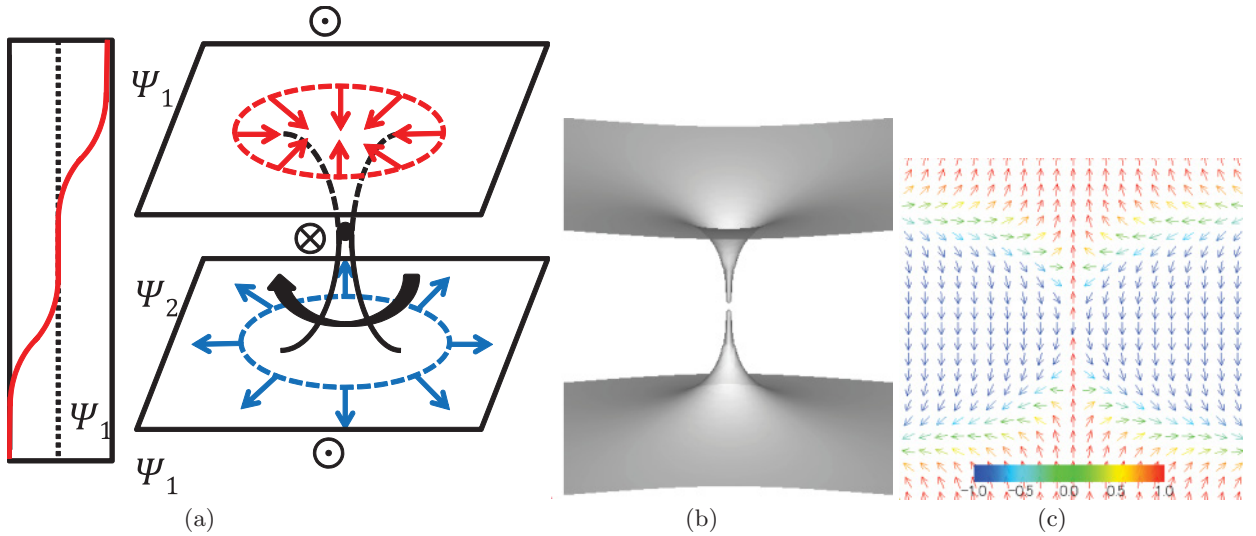

FIG. 9. (Color online) (a) A pair of a D-brane (domain wall) and an anti-D-brane (antidomain wall) stretched by a string (vortex) in two-component BECs. The branes are perpendicular to the x^1 axis and the string is placed along the x^1 axis. The arrows denote pseudospins. The Ψ_1 (Ψ_2) component is filled outside (between) the branes, where the other component is zero. In the upper (lower) region outside the branes, the phase of Ψ_1 is fixed to be zero (π). In the middle region, the phase of Ψ_2 has winding around the vortex placed at the x^1 axis. Accordingly, the pseudospin rotates once (anti)clockwise at the endpoint of string on the (anti)brane. The profile of the Ψ_1 component along a line parallel to the x^1 axis at $(x^2,x^3) \neq 0$ represents two kinks in the left panel, while the profile of the Ψ_1 component along the x^1 axis shows the coincident two kinks, that is, a dark soliton. The dot in the center denotes the point $(\Psi_1,\Psi_2) = 0$, which corresponds to a singularity in the NLσM approximation ($\rho = $ const) in (b). (b) The isosurface of $s_3 = 0$ of an approximate solution in Eq. (30) with a domain wall and an antidomain wall stretched by a vortex in the O(3) NLσM, where $M = 1$, $x_1^1 = -3$, $x_2^1 = 3$, $\phi_1 = 0$, $\phi_2 = \pi$. (c) The pseudospin texture of an approximate solution in Eq. (30).

Here x_1^1 and x_2^1 ($x_1^1 < x_2^1$) represent the positions of the wall and antiwall, respectively, while ϕ_1 and ϕ_2 denote the phase of the wall and antiwall, respectively. This solution is good when the distance $|x_1^1 - x_2^2|$ between the walls is large compared with the mass scale M^{-1}. For our purpose, the phases are taken as $\phi_1 = \phi_2 + \pi$, which means that the Ψ_1 component has a dark soliton when the intermediate Ψ_2 component vanishes. The isosurface of $s_3 = 0$ and the pseudospin structure of this configuration are plotted in Figs. 9(b) and 9(c), respectively. In order to avoid the logarithmic bending of the walls, one can use $u_v(z)$ in Eq. (29) with $N_{v_1} = N_{v_2}$ instead of Eq. (32), as in Fig. 10. The solution in Eqs. (30)–(32) of the O(3) NLσM has a singularity at the midpoint of the vortex stretching the domain walls, as in Fig. 9. It is, however, merely an artifact in the NLσM approximation of $\rho = $ const; the singularity does not exist in the original theory without such the approximation, because ρ varies and merely vanishes at that point.

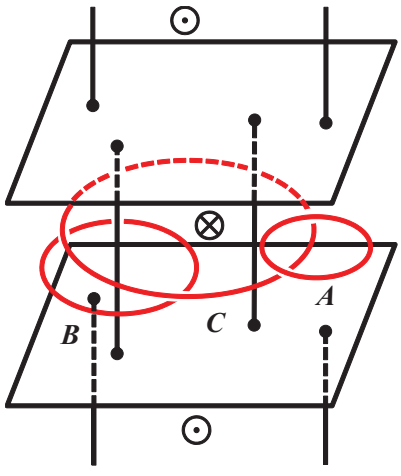

FIG. 10. (Color online) Loops in the wall-vortex systems. While the loop A yields an untwisted vortex ring in Fig. 11(a), the loop B (C) yields a vorton, that is, a vortex ring twisted once (twice). A vorton with twisted once is shown in Fig. 11(b).

Now let us discuss the dynamics of the wall-antiwall configuration. As in the case without a stretched string, the configuration itself is unstable to decay, and vortex loops are created in the Ψ_1 component. Since the Ψ_2 component is localized along the vortex core, the $s_3 = 0$ surface forms a torus (ring), where the region of $s_3 > 0$ is outside the torus, whereas the region $s_3 < 0$ is inside it. As far as the phase of Ψ_2 component inside the ring is concerned, the vortex loops are classified into (1) the untwisted case [see Fig. 11(a)] and (2) the twisted case [see Fig. 11(b)].

(1) If the closed vortex loop encloses no stretched vortices as the loop A in Fig. 10, the vortex loop is not twisted, as in Fig. 11(a). Equivalently, the phase of the Ψ_2 component inside the ring is not wound.

(2) However, if the vortex loop encloses n stretched vortices as the loops B and C in Fig. 10, the vortex loop is twisted n times. It implies that the phase of the Ψ_2 component inside the ring is wound n times. A vortex loop twisted once, which is nothing but a vorton with the minimum twist, is shown in Fig. 11(b). The vertical section of the torus by the x^1-x^2 plane is a pair of a skyrmion (coreless vortex) and an antiskyrmion (coreless vortex). Moreover, the presence of the stretched vortex implies that the phase winds anticlockwise along the loops, as can be seen by the arrows on the top and the bottom

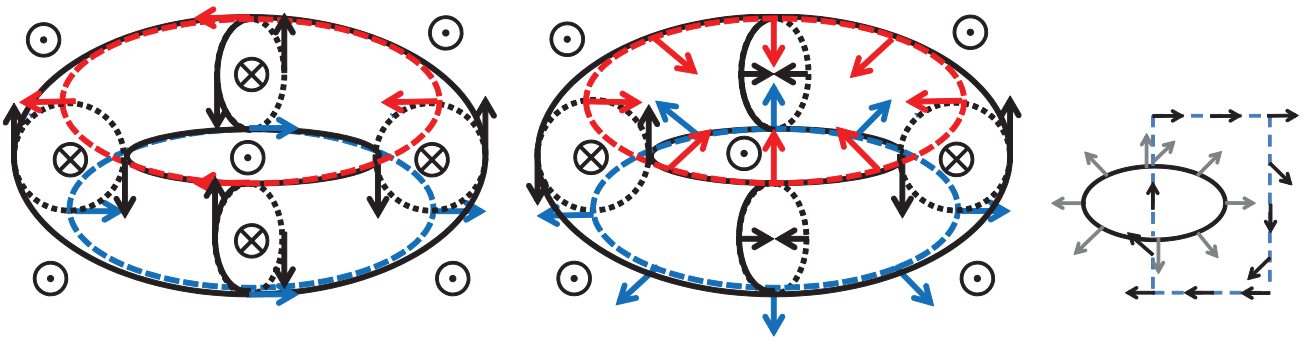

FIG. 11. (Color online) (a) The pseudospin texture of an untwisted vortex ring, and (b) and (c) the pseudospin and phase textures of a twisted vortex ring, that is, a vorton, after the brane-antibrane annihilation. (b) The pseudospin structure of the vorton. The torus divides the regions of Ψ_1 and Ψ_2 which repel each other: Ψ_1 (Ψ_2) are filled outside (inside) the torus. The vertical section of the torus by the x^1-x^2 plane is a pair of 2D skyrmions and antiskyrmions. While they rotate along the x^1 axis their pseudospins are twisted. This spin texture is equivalent to that of a knot [22,28,29]. (c) The phase structure of the vorton. The arrows denote the phase of Ψ_1 and Ψ_2. The circle denotes the core of vorton where Ψ_2 is filled and Ψ_1 is zero. The phase of Ψ_2 winds once along that circle. The square of the dotted line denotes a loop where Ψ_2 is zero. The phase of Ψ_1 winds once along that loop. Note that the loops of Ψ_1 and Ψ_2 are zero, respectively, make a link. Along the zeros of Ψ_1 (Ψ_2), the phase of Ψ_2 (Ψ_1) winds once.

of the torus in Fig. 11(b). When the 2D skyrmion pair rotate along the x^1 axis their phases are twisted and connected to each other at the π rotation. Note that the zeros of Ψ_1 and Ψ_2 make a link. Along the zeros of Ψ_1 (Ψ_2), the phase of Ψ_2 (Ψ_1) winds once. The configuration is nothing but a vorton.

It may be interesting to point out that this spin texture is equivalent to the one of a knot soliton [22,28,29], that is, a topologically nontrivial texture with a Hopf charge $\pi_3(S^2) \simeq \mathbf{Z}$ in an O(3) NLσM. Mathematically, this fact implies that a vorton is Hopf fibered over a knot.

Finally, to confirm a vorton creation of a domain wall pair annihilations, we show a numerical simulation of the time-dependent GP equation $i\hbar\partial_t\Psi_j = \delta E/\delta\Psi_j^*$ for the domain wall pair with a stretched vortex in Fig. 12. The numerical scheme to solve the GP equation is a Crank-Nicholson method with the Neumann boundary condition in a cubic box without external potentials. The box size is $52.1\xi \times 52.1\xi \times 52.1\xi$ with $\xi = \hbar/\sqrt{m\mu_1}$. We prepare a pair of a domain wall and an antidomain wall at coincident limit with a vortex winding in the Ψ_2 component. Here, for simplicity we put a cylindrically symmetric perturbation, which is expected to be induced from various modes of the string. Several holes grow after being created, and there appear vortex loops. Although the holes appear asymmetrically because of the cubic boundary, the boundary effect is small in the center region and the initial perturbation causes a vortex loop there. The vortex loop enclosing the Ψ_2 winding, which is nothing but a vorton, is created in the center of Fig. 12(c).

C. Equivalence of the vorton to the three-dimensional skyrmion

It has been already shown in [8,9] that 3D skyrmions are topologically equivalent to vortons in two-component BECs. In this section we show it in our context of the brane-antibrane annihilations.

In Fig. 13 the arrows denote the phase of Ψ_1 along a large loop (of the square of the dotted line) going to the boundary where Ψ_2 is zero, making a link with the vorton core. The

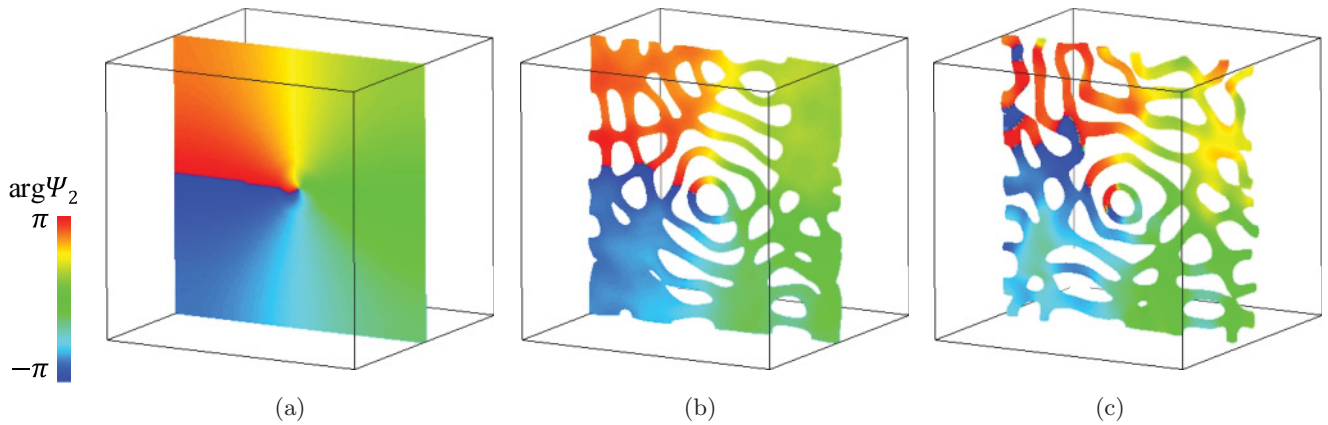

FIG. 12. (Color online) A numerical simulation of a vorton creation. Surfaces are defined by $n_1 - n_2 = 0.18(\mu_1/g)$ ($\mu_1 = g = 1, \hbar = m = 1$), while color represents the phase of the Ψ_2 component. (a) First, we prepare a pair of a domain wall and an antidomain wall at coincident limit with a vortex winding in the Ψ_2 component. (b) Holes are created in the wall annihilation. (c) A vorton is created in the center.

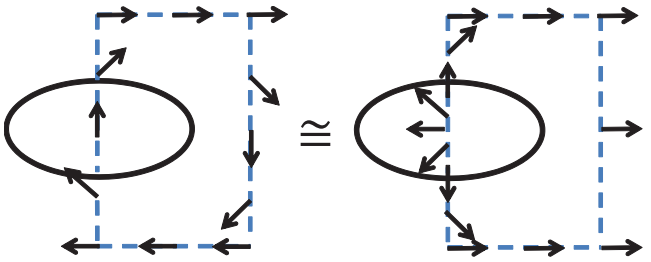

FIG. 13. (Color online) The equivalence between the vorton and the 3D skyrmion. The arrows denote the phase of Ψ_1 along a large loop (of the square of the dotted line) going to the boundary where Ψ_2 is zero, making a link with the vorton core. The left panel represents the configuration of the vorton from the brane-antibrane annihilation [see Fig. 11(a)], while the right panel represents the configuration of a 3D skyrmion. They are topologically isomorphic to each other.

left panel of Fig. 13 represents the phases of Ψ_1 and Ψ_2 of the vorton from the brane-antibrane annihilation [see also Fig. 11(b)]. This is topologically equivalent to the right panel of Fig. 13. Here we show that the phase structure of the right panel is that of a 3D skyrmion. They are topologically isomorphic to each other.

First, let us introduce the matrix U as

$$\begin{pmatrix}\Psi_1\\ \Psi_2\end{pmatrix} = \begin{pmatrix}\Psi_1 & -\Psi_2^*\\ \Psi_2 & \Psi_1^*\end{pmatrix}\begin{pmatrix}1\\ 0\end{pmatrix} = U\begin{pmatrix}1\\ 0\end{pmatrix}, \tag{33}$$

with

$$U \equiv \begin{pmatrix}\Psi_1 & -\Psi_2^*\\ \Psi_2 & \Psi_1^*\end{pmatrix} \tag{34}$$

being an element of an SU(2) group, when

$$\det U = |\Psi_1|^2 + |\Psi_2|^2 = 1. \tag{35}$$

The GP energy functional given in Eq. (5) is not SU(2) symmetric in general. When the relations

$$g_{11} = g_{22} = g_{12}, \quad \mu_1 = \mu_2 \tag{36}$$

hold, the GP energy functional is SU(2) symmetric, and Eq. (35) holds (up to overall constant) [47].

Even when the GP energy functional given in Eq. (5) is not SU(2) symmetric, we can approximately consider the parametrization by U in Eq. (34). A rotationally symmetric configuration of a 3D skyrmion can be given by [6]

$$U = \exp i\left(f(r)\frac{\mathbf{r}}{|\mathbf{r}|}\cdot\sigma\right) \tag{37}$$

with a function $f(r)$ with the boundary condition

$$f(r=0) = n\pi, \quad f(r=R) = 0, \tag{38}$$

where R is the size of the system. Here, $n \in \mathbf{Z}$ is an element of the third homotopy group $\pi_3(\mathrm{SU}(2)) \simeq \mathbf{Z}$.

In the polar coordinates (r,θ,ϕ),

$$\frac{\mathbf{r}}{|\mathbf{r}|} = (\sin\theta\cos\phi, \sin\theta\sin\phi, \cos\theta). \tag{39}$$

By using the formula $\exp(i\Theta\mathbf{n}\cdot\sigma) = \cos\Theta + i\mathbf{n}\cdot\sigma\sin\Theta$ for $\mathbf{n}^2 = 1$, the 3D skyrmion in Eq. (33) with U in Eq. (37) can be obtained as

$$\begin{pmatrix}\Psi_1\\ \Psi_2\end{pmatrix} = \begin{pmatrix}\cos f(r) - i\sin f(r)\cos\theta\\ \sin f(r)\sin\theta e^{-i\phi}\end{pmatrix}. \tag{40}$$

First, let us study the phase structure of Ψ_1 of the 3D skyrmion in Eq. (40). At the boundaries and the origin, Eq. (40) becomes

$$\begin{aligned}\begin{pmatrix}\Psi_1\\ \Psi_2\end{pmatrix} &= \begin{pmatrix}1\\ 0\end{pmatrix} \quad \text{at} \quad r = R,\\ \begin{pmatrix}\Psi_1\\ \Psi_2\end{pmatrix} &= \begin{pmatrix}(-1)^n\\ 0\end{pmatrix} \quad \text{at} \quad r = 0.\end{aligned} \tag{41}$$

Along the x^1 axis ($\theta = 0,\pi$), Eq. (40) becomes

$$\begin{aligned}\begin{pmatrix}\Psi_1\\ \Psi_2\end{pmatrix} &= \begin{pmatrix}\exp[-if(r)]\\ 0\end{pmatrix} \quad \text{at} \quad \theta = 0,\\ \begin{pmatrix}\Psi_1\\ \Psi_2\end{pmatrix} &= \begin{pmatrix}\exp[if(r)]\\ 0\end{pmatrix} \quad \text{at} \quad \theta = \pi,\end{aligned} \tag{42}$$

Eqs. (41) and (42) show, in the case of $n = 1$, the phase structure of Ψ_1 in the right panel of Fig. 13.

Second, let us study the phase structure of Ψ_2. We consider the ring defined by $\theta = \pi/2$ and the radius r such that $f(r) = \pi/2$. Along this ring, the Ψ_i are

$$\begin{pmatrix}\Psi_1\\ \Psi_2\end{pmatrix} = \begin{pmatrix}0\\ e^{-i\phi}\end{pmatrix}. \tag{43}$$

The Ψ_2 component winds once along this ring, as in Fig. 11(c). This winding of the Ψ_2 component originates from the winding in the brane-antibrane configuration in Eq. (32).

We thus have seen that the 3D skyrmion in Eq. (33) is topologically equivalent to a vorton.

V. SUMMARY AND DISCUSSION

We have studied a mechanism to create a vorton or three-dimensional skyrmion in phase separated two-component BECs. We consider a pair of a domain wall and an antidomain wall with vortices stretched between them. The Ψ_2 component is sandwiched by the regions of the Ψ_1 component, where the phase difference of Ψ_1 in the two separated regions is taken to be π. When the domain wall pair decays, there appear vortex loops of the Ψ_1 component with the Ψ_2 component trapped inside their cores. If a Ψ_1 vortex loop encloses one stretched vortex, it becomes a vorton. More generally, if the vortex loop encloses n of the stretched vortices, it becomes a vortex ring with the phase of Ψ_2 twisted n times. We also have confirmed that the vorton ($n = 1$) is topologically equivalent to a 3D skyrmion.

Experimentally this can be realized by preparing the phase separation in the order Ψ_1, Ψ_2, and Ψ_1 components, and rotating the intermediate Ψ_2 component. By selectively removing the filling Ψ_2 component with a resonant laser beam, the collision of the brane and antibrane can be made, to create vortons.

Once created in the laboratory, one can study the stability and dynamics of a vorton experimentally. The vorton will propagate along the direction perpendicular to the initial configuration of the branes. Therefore, to investigate the dynamics of a vorton, we need to prepare a large size of cloud in that

direction. In the case of untwisted vortex loop (usual loop, not a vorton), it will easily shrink and eventually decay into phonons if the thermal dissipation works enough. However, the vorton should be stable against the shrinkage and will propagate to reach the surface of the atomic cloud. Such a difference must be a benchmark to detect vortons in experiments.

On the other hand, the thermal and quantum fluctuations may make the vorton *unstable*. Our numerical calculations rely on the mean field GP theory. The topological charge of a vorton is the winding of the phase of Ψ_2 along the closed loop (which is proportional to the superflow along the closed loop). Since this topological charge is defined only in the vicinity of the vorton, there is a possibility that it can be unwound, once quantum and thermal fluctuation is taken into account beyond the mean-field theory. Quantum mechanically, such a decay is caused by an instanton effect (quantum tunneling). This process also resembles the phase slip of superfluid rings. The vorton decay by the quantum and thermal tunneling is considered to be an important process in high energy physics and cosmology since it will radiate high energy particles such as photons, which may explain some high energy astrophysical phenomena observed in our Universe. Therefore it would be important that one realizes vortons in laboratory by using ultracold atomic gases; it may simulate a vorton decay with emitting phonons quantum mechanically, beyond the mean-field approximation.

In this paper we have mainly studied topological aspects of the vorton creation using the NLσM approximation. In order to study dynamics of topological defects beyond this approximation, we need a precise form of the interaction between the defects. An analytic form of the interaction between vortices was derived in the case of miscible ($c_2 > 0$) two-component BECs, and it was applied to the analysis of vortex lattices [48]. Extension to the case of the immiscible case ($c_2 < 0$) focused in this paper will be useful to study the interaction between vortices attached to domain walls, and that between vortons and/or walls.

In our previous paper [38] we discussed that the domain wall in two-component BECs can be regarded as a D2-brane, as the D-brane soliton [30–34] in field theory, where "Dp-brane" implies a D-brane with p space dimensions. This is because the string endpoints are electrically charged under U(1) gauge field of the Dirac-Born-Infeld (DBI) action for a D-brane [49]. In our context, the U(1) gauge field is obtained by a duality transformation from U(1) Nambu-Goldstone mode of the domain wall. Since the D-brane soliton [38] in two-component BECs, precisely coincides with a BIon [50], that is, a soliton solution of the DBI action of a D-brane, the domain wall can be regarded as a D2-brane.

On the other hand, it is known in string theory [44] that when a Dp-brane and an anti-Dp-brane annihilate on collision, there appear D$(p-2)$ branes. If we want to regard our domain wall as a D2-brane, the pair annihilation of a D2-brane and anti-D2-brane should result in the creation of D0-branes. Therefore, a discussion along this line leads us to suggest a possible interpretation of 3D skyrmions as D0-branes, which are point-like objects.

ACKNOWLEDGMENTS

M.N. would like to thank Michikazu Kobayashi for a useful discussion on three-dimensional skyrmions. This work was supported by KAKENHI from JSPS (Grants No. 21340104, No. 21740267, and No. 23740198). This work was also supported by the "Topological Quantum Phenomena" (No. 22103003 and No. 23103515) Grant-in Aid for Scientific Research on Innovative Areas from the Ministry of Education, Culture, Sports, Science and Technology (MEXT) of Japan.

[1] E. Witten, Nucl. Phys. B **249**, 557 (1985).
[2] R. L. Davis and E. P. S. Shellard, Phys. Lett. B **209**, 485 (1988).
[3] E. Radu and M. S. Volkov, Phys. Rep. **468**, 101 (2008).
[4] G. E. Volovik, *The Universe in a Helium Droplet* (Clarendon, Oxford, 2003).
[5] A. Vilenkin and E. P. S. Shellard, *Cosmic Strings and Other Topological Defects*, Cambridge Monographs on Mathematical Physics (Cambridge University Press, Cambridge, 2000).
[6] T. H. R. Skyrme, Proc. R. Soc. London Ser. A **260**, 127 (1961); Nucl. Phys. **31**, 556 (1962).
[7] N. S. Manton and P. Sutcliffe, *Topological Solitons* (Cambridge University Press, Cambridge, 2004), p. 493.
[8] J. Ruostekoski and J. R. Anglin, Phys. Rev. Lett. **86**, 3934 (2001).
[9] R. A. Battye, N. R. Cooper, and P. M. Sutcliffe, Phys. Rev. Lett. **88**, 080401 (2002).
[10] U. A. Khawaja and H. T. C. Stoof, Nature (London) **411**, 918 (2001); Phys. Rev. A **64**, 043612 (2001).
[11] C. M. Savage and J. Ruostekoski, Phys. Rev. Lett. **91**, 010403 (2003).
[12] J. Ruostekoski, Phys. Rev. A **70**, 041601 (2004).
[13] S. Wuester, T. E. Argue, and C. M. Savage, Phys. Rev. A **72**, 043616 (2005).
[14] I. F. Herbut and M. Oshikawa, Phys. Rev. Lett. **97**, 080403 (2006); A. Tokuno, Y. Mitamura, M. Oshikawa, and I. F. Herbut, Phys. Rev. A **79**, 053626 (2009).
[15] M. A. Metlitski and A. R. Zhitnitsky, J. High Energy Phys. 06 (2004) 017.
[16] P. F. Bedaque, E. Berkowitz, and S. Sen, e-print arXiv:1111.4507.
[17] L. S. Leslie, A. Hansen, K. C. Wright, B. M. Deutsch, and N. P. Bigelow, Phys. Rev. Lett. **103**, 250401 (2009); J. Y. Choi, W. J. Kwon, and Y. I. Shin, *ibid.* **108**, 035301 (2012).
[18] H. T. C. Stoof, E. Vliegen, and U. Al Khawaja, Phys. Rev. Lett. **87**, 120407 (2001).
[19] J.-P. Martikainen, A. Collin, and K.-A. Suominen, Phys. Rev. Lett. **88**, 090404 (2002).
[20] C. M. Savage and J. Ruostekoski, Phys. Rev. A **68**, 043604 (2003).
[21] V. Pietilä and M. Möttönen, Phys. Rev. Lett. **103**, 030401 (2009).
[22] Y. Kawaguchi, M. Nitta, and M. Ueda, Phys. Rev. Lett. **100**, 180403 (2008).
[23] G. W. Semenoff and F. Zhou, Phys. Rev. Lett. **98**, 100401 (2007); M. Kobayashi, Y. Kawaguchi, M. Nitta, and M. Ueda, *ibid.* **103**, 115301 (2009).

[24] K. Kasamatsu, M. Tsubota, and M. Ueda, Int. J. Mod. Phys. B **19**, 1835 (2005); Y. Kawaguchi, M. Kobayashi, M. Nitta, and M. Ueda, Prog. Theor. Phys. Suppl. **186**, 455 (2010); M. Ueda and Y. Kawaguchi, e-print arXiv:1001.2072.
[25] G. Thalhammer, G. Barontini, L. DeSarlo, J. Catani, F. Minardi, and M. Inguscio, Phys. Rev. Lett. **100**, 210402 (2008).
[26] S. B. Papp, J. M. Pino, and C. E. Wieman, Phys. Rev. Lett. **101**, 040402 (2008).
[27] K. Kasamatsu, M. Tsubota, and M. Ueda, Phys. Rev. A **71**, 043611 (2005).
[28] E. Babaev, L. D. Faddeev, and A. J. Niemi, Phys. Rev. B **65**, 100512 (2002).
[29] E. Babaev, Phys. Rev. B **79**, 104506 (2009).
[30] J. P. Gauntlett, R. Portugues, D. Tong, and P. K. Townsend, Phys. Rev. D **63**, 085002 (2001).
[31] M. Shifman and A. Yung, Phys. Rev. D **67**, 125007 (2003).
[32] Y. Isozumi, M. Nitta, K. Ohashi, and N. Sakai, Phys. Rev. D **71**, 065018 (2005).
[33] M. Eto, Y. Isozumi, M. Nitta, K. Ohashi, and N. Sakai, J. Phys. A **39**, R315 (2006).
[34] M. Eto, T. Fujimori, T. Nagashima, M. Nitta, K. Ohashi, and N. Sakai, Phys. Rev. D **79**, 045015 (2009).
[35] J. Polchinski, Phys. Rev. Lett. **75**, 4724 (1995).
[36] R. G. Leigh, Mod. Phys. Lett. A **4**, 2767 (1989).
[37] J. Polchinski, *String Theory* (Cambridge University Press, Cambridge, 1998).
[38] K. Kasamatsu, H. Takeuchi, M. Nitta, and M. Tsubota, J. High Energy Phys. 11 (2010) 068.
[39] M. O. Borgh and J. Ruostekoski, e-print arXiv:1202.5679.
[40] D. I. Bradley, S. N. Fisher, A. M. Guénault, R. P. Haley, J. Kopu, H. Martin, G. R. Pickett, J. E. Roberts, and V. Tsepelin, Nat. Phys. **4**, 46 (2008).
[41] B. P. Anderson, P. C. Haljan, C. A. Regal, D. L. Feder, L. A. Collins, C. W. Clark, and E. A. Cornell, Phys. Rev. Lett. **86**, 2926 (2001).
[42] H. Takeuchi, K. Kasamatsu, M. Nitta, and M. Tsubota, J. Low Temp. Phys. **162**, 243 (2011); H. Takeuchi, K. Kasamatsu, M. Tsubota, and M. Nitta, arXiv:1205.2330 [cond-mat.quant-gas].
[43] C. J. Pethick and H. Smith, *Bose-Einstein Condensation in Dilute Gases*, 2nd ed. (Cambridge University Press, Cambridge, 2008).
[44] A. Sen, Int. J. Mod. Phys. A **20**, 5513 (2005).
[45] P. W. Anderson and G. Toulouse, Phys. Rev. Lett. **38**, 508 (1977).
[46] A. M. Polyakov and A. A. Belavin, JETP Lett. **22**, 245 (1975) [Pisma Zh. Eksp. Teor. Fiz. **22**, 503 (1975)].
[47] In the SU(2) symmetric case, the conditions in Eq. (36) imply $c_1 = c_2 = 0$ in the O(3) NLσM description, and consequently there is no potential. By noting the isomorphism SU(2) $\simeq S^3$, the target space S^2 is a quotient of S^3 by gauge symmetry $S^2 = S^3/\mathrm{U}(1)$, which is nothing but the Hopf fiberation.
[48] M. Eto, K. Kasamatsu, M. Nitta, H. Takeuchi, and M. Tsubota, Phys. Rev. A **83**, 063603 (2011); P. Mason and A. Aftalion, *ibid.* **84**, 033611 (2011); A. Aftalion, P. Mason, and J. Wei, *ibid.* **85**, 033614 (2012).
[49] P. A. M. Dirac, Proc. R. Soc. London Ser. A **268**, 57 (1962); M. Born and L. Infeld, *ibid.* **144**, 425 (1934).
[50] G. W. Gibbons, Nucl. Phys. B **514**, 603 (1998); C. G. Callan and J. M. Maldacena, *ibid.* **513**, 198 (1998).